The Institute of Space and Astronautical Science
Report SP No. 17 March 2003

Viscous Shock Layer Studies of a Super Orbital Reentry Capsule Using a Multi Vibrational Temperature Model

By

Ryouji DOIHARA*, and Michio NISHIDA†

(1 February 2003)

Abstract: Numerical studies of the shock layer of a super orbital reentry capsule have been conducted by using thermochemical nonequilibrium VSL (Viscous Shock Layer) equations. In the present analysis, vibrational temperature has been treated as individual molecular species vibrational temperature. The analysis has been performed for the MUSES-C reentry conditions, and the temperatures and chemical species mole fractions in the shock layer have been revealed for the typical reentry altitudes of 84 km and 64 km. Radiative heat flux and spectra have been also computed from the results of the VSL analysis to discuss the necessity of the multi vibrational temperature model. Finally, convective heat fluxes for the multi vibrational temperature model and three temperature model are compared.

1. INTRODUCTION

The atmospheric entry speed of the MUSES-C capsule is over 12 km/s, so that a very strong shock wave is generated around the capsule, whereby the shock layer gas is much more highly heated than the case of a normal earth orbital reentry. Hence, radiative heat flux is expected to be stronger in the super orbital reentry.

Typical feature in the super orbital reentry is an increase in radiative heat transfer to the capsule, which will be of the order comparable to convective heat transfer. More accurate prediction of the radiative heat transfer requires more accurate analysis of temperatures, in particular the detailed analysis of vibrational temperature, because the intensity of band spectrum is dependent on vibrational temperature. On the view of this point, vibrational temperature is treated as individual molecular-species vibrational temperature in the present analysis.

The present computation uses the VSL (Viscous Shock Layer) method, which is a space marching method. This method is more beneficial, because unlike a time marching numerical

* Department of Aeronautics and Astronautics, Fukuoka 812-8581, JAPAN.
Present address: Fluid Flow Division, Metrology Institute of Japan, National Institute of Advanced Industrial Science and Technology, Tsukuba 305-8563, JAPAN.
† Department of Aeronautics and Astronautics, Fukuoka 812-8581, JAPAN.

method, it has the advantage of smaller computational time. Even though the VSL method is limited to the analysis of a shock layer, this method has been extensively employed in the past to analyze the hypersonic flow around a space transportation vehicle during atmospheric entry (Miner and Lewis 1975, Gupta et al. 1990a, Gupta et al. 1990b, Sakamura & Nishida 1991, Nishida & Sakamura 1994, Gupta et al. 1996, Suzuki et al. 1996, Doihara & Nishida 2001, Doihara & Nishida 2002). In these studies, a multi vibrational temperature model has not been utilized. In the present analysis, thermochemical nonequilibrium viscous shock layer (VSL) equations are extended to a multi vibrational temperature model apply to the shock layer studies of the MUSES-C reentry capsule. Thereby spectral characteristics and radiative heat flux can be analyzed in more detail. The radiation analysis is conducted by using the 'SPRADIAN' code developed by Fujita & Abe (1997).

2. NUMERICAL ANALYSIS

2.1 Flow and Thermochemical Model

In the present analysis, the following assumptions are introduced:

1) The flowfield is a high temperature thermochemical nonequilibrium shock layer, that includes eleven species (N_2, O_2, NO, N, O, N_2^+, O_2^+, NO^+, N^+, O^+, e^-).
2) The flow is treated as axisymmetric and steady.
3) A thermal nonequilibrium with five temperatures is introduced: translational-rotational temperature (T), vibrational temperatures of individual molecular species ($T_{\mathrm{vib,N_2}}$, $T_{\mathrm{vib,O_2}}$, $T_{\mathrm{vib,NO}}$) and electron-electronic temperature (T_e). Vibrational temperature of molecular ion species is set to being equal to that of corresponding neutral species.
4) Electronic temperatures of N, N^+, O, O^+, O_2 are equal and fully equilibrated with electron temperature. These species have low-lying electronic states and so only two low-lying electronic states of them are considered (Park 1990). Although N_2^+ also has a low-lying first excitation state, it is not considered in the analysis because of its small fraction. The first excitation state of N_2, NO, O_2^+ and NO^+ are very high, so that they are scarcely populated at this state.
5) Emission and absorption of radiation are not considered in the VSL calculation.

2.2 Governing Equations and Boundary Conditions

The configuration of the MUSES-C reentry capsule is given by a hyperboloid with a 0.2 m nose radius and a 45° semi-apex angle (Fig. 1). The governing equations are the full viscous shock layer (FVSL) equations written for the coordinates shown in Fig. 1. They are formulated for a multi component gas flow in thermochemical nonequilibrium, which are composed of equations of species mass conservation, over-all momentum, translational-rotational energy, each molecular species vibrational energy and electron-electronic energy. The VSL equations are obtained from the steady-state Navier-Stokes equations by retaining terms up to the second order in the Reynolds number parameter ϵ defined by $\epsilon = \sqrt{\mu_\mathrm{ref}/\rho_\infty U_\infty R_\mathrm{n}}$ where μ_ref is the viscosity evaluated at the reference temperature $T_\mathrm{ref} = U_\infty^2/C_{p,\infty}$, ρ_∞ is the free stream density, U_∞ is the free stream speed, R_n is the nose radius of a body and $C_{p,\infty}$ is the specific heat in the free stream. In this study, the value of ϵ^3 is of the orders of 10^{-2} to 10^{-4} for the altitudes of interest for this study (90 km - 60 km), so that the VSL analysis can be expected to provide sufficiently accurate results.

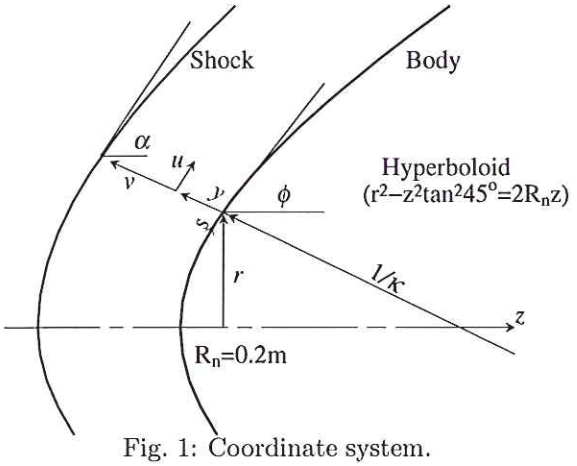

Fig. 1: Coordinate system.

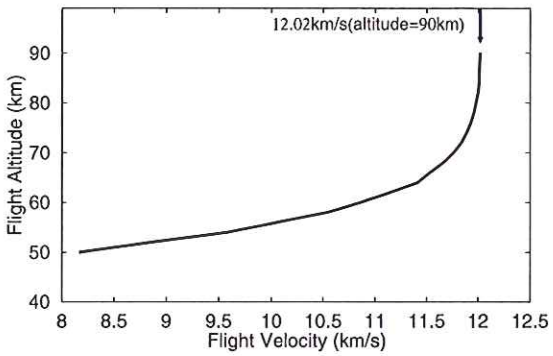

Fig. 2: Reentry trajectory of MUSES-C.

Boundary conditions are imposed as described below. At the wall, no-slip conditions ($u = v = 0$) are imposed. The wall temperature $T_{\rm w}$ is assumed to be constant at 2,500 K. An isothermal wall is assumed at each altitude, and the vibrational temperature on the wall is considered to be the wall temperature. The boundary condition for electron temperature is calculated by Eq.(10) in Nishida (1972) that was derived from the Langmuir probe theory. Species wall boundary conditions are determined by either noncatalytic wall (NCW) condition or fully catalytic wall (FCW) condition:

$$\left(\frac{\partial C_i}{\partial y}\right)_{\rm w} = 0 \quad \text{(NCW)}, \qquad C_{i,{\rm w}} = C_{i_\infty} \quad \text{(FCW)}$$

where C_i is the mass concentration of species i, y is the coordinate normal to the wall, subscripts w and ∞ denote, respectively, wall and free stream.

Boundary conditions immediately behind the shock are given by shock jump conditions from the free stream conditions for the reentry trajectory (Fig. 2). Low density gas effect was included into the analysis with shock slip conditions (Miner & Lewis 1975). Vibrational temperature and electron temperature immediately behind the shock are set to being equal to the free stream temperature.

2.3 Transport properties

The transport properties (viscosity, thermal conductivity, diffusion coefficient) are evaluated by extending Yos' formula, which is based on the first Chapman-Enskog approximation, to a multi temperature gas mixture (Gupta et al. 1990). The diffusion coefficients of Curtiss and Hirschfelder (1949) are used, and ambipolar diffusion is assumed for ions.

2.4 Internal Energy Exchange

The energy transfers considered here are translation-vibration, translation-electron, rotation-electron, vibration-vibration and vibration-electron, as shown in Fig. 3.

The energy transfer rate between translation and vibration is derived from the formula of the Landau-Teller model. The vibrational relaxation time is evaluated by an empirical formula of Millikan & White (1963) and the correction term of Park's collision limit (Park 1985). The translation-electron and rotation-electron energy transfer rates are taken from Lee (1985), and Lazdinis & Petrie (1974), respectively.

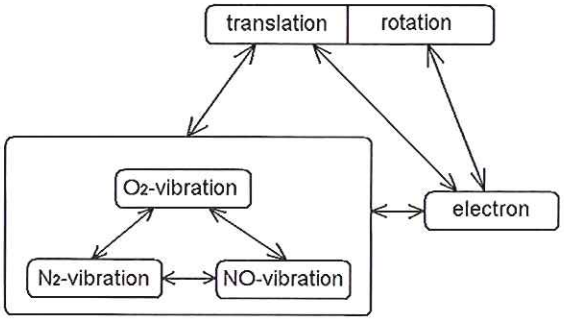

Fig. 3: Internal energy transfer.

The relaxation time for the energy exchange between nitrogen vibration and electron (τ_{N_2-e}) is taken from Lee (1992). The relaxation times for NO and O_2 ($\tau_{O_2-e}, \tau_{NO-e}$) are evaluated from the nitrogen relaxation time by using the ratios of the characteristic temperature for vibration, $\Theta_{vib,N_2}/\Theta_{vib,O_2} = 1.492$ and $\Theta_{vib,N_2}/\Theta_{vib,NO} = 1.239$ (Park 1990):

$$\tau_{O_2-e} = 300 \times \tau_{N_2-e}(1.492T_e) \quad (1)$$

$$\tau_{NO-e} = 300 \times \tau_{N_2-e}(1.239T_e) \quad (2)$$

The factor 300 accounts for the fact that the electron-vibration energy transfer cross sections for O_2 and NO are considered to be much less than that of N_2 (Park 1990). The vibration-vibration energy exchange rates are taken from Candler & MacCormack (1991).

An average vibrational energy removed by dissociation is very important in a super orbital reentry speed range. In the present study, the CVDV model (Treanor & Marrone 1962) is employed to describe such an energy loss. Let $Q_{D,i}$ be the vibrational energy loss of species i due to dissociation and $Q_{R,i}$ be the energy gain due to recombination and then we have

$$Q_{D,i} = \left[\frac{k\Theta_{vib,i}}{\exp\left(\Theta_{vib,i}T_{m,i}\right)-1} - \frac{kN_i\Theta_{vib,i}}{\exp\left(N_i\Theta_{vib,i}T_{m,i}\right)-1}\right], \quad (3)$$

$$Q_{R,i} = \left[\frac{1}{2}\left(N_i-1\right)k\Theta_{vib,i}\right], \quad (4)$$

where k is the Boltzmann constant, $\Theta_{vib,i}$ is the characteristic temperature for vibration of molecular species i, N_i is the fractional number of a vibrator. $T_{m,i}$ is given below,

$$\frac{1}{T_{m,i}} = \frac{1}{T_{vib,i}} - \frac{1}{T}. \quad (5)$$

2.5 Air Chemistry

An 11 species air model consisting of $N_2, O_2, NO, N, O, NO^+, O^+, N^+, N_2^+, O_2^+$ and e^- is adopted here (76.5 % N_2 + 23.5 % O_2 in the free stream). Air chemistry considered here is shown in Table 1, and chemical reaction rates are such that the Park's model (Park 1993) is extended to a multi vibrational temperature model. Rate constants are assumed to be a function of controlling temperatures T_f and T_b depending on the type of reaction, and they are given by the following expressions:

$$k_{f,r}(T_{f,r}) = C_r T_{f,r}^{s_r}\exp(-\theta_r/T_{f,r}), \quad k_{b,r}(T_{b,r}) = k_{f,r}(T_{b,r})/K_r^{eq}(T_{b,r}) \quad (6)$$

where $k_{\mathrm{f},r}$ and $k_{\mathrm{b},r}$ are the forward and backward reaction rate coefficients for reaction r, respectively. Likewise $T_{\mathrm{f},r}$ and $T_{\mathrm{b},r}$ are the forward and backward controlling temperatures for reaction r, respectively. The controlling temperatures are shown in Table. 1. The values of C_r, s_r and θ_r can be obtained from Park (1993).

Table 1: Air chemistry.

r	Reactants		Products	T_f	T_b	r	Reactants		Products	T_f	T_b
1	$N_2 + M_1^a$	$\rightleftarrows$	$N + N + M_1$	$\sqrt{T \cdot T_{\mathrm{vib,N_2}}}$	T	13	$NO^+ + O$	$\rightleftarrows$	$N^+ + O_2$	T	T
2	$N_2 + M_2^b$	$\rightleftarrows$	$N + N + M_2$	$\sqrt{T \cdot T_{\mathrm{vib,N_2}}}$	T	14	$O_2^+ + N$	$\rightleftarrows$	$N^+ + O_2$	T	T
3	$N_2 + e^-$	$\rightleftarrows$	$N + N + e^-$	T_e	T_e	15	$NO + O^+$	$\rightleftarrows$	$N^+ + O_2$	T	T
4	$O_2 + M_1$	$\rightleftarrows$	$O + O + M_1$	$\sqrt{T \cdot T_{\mathrm{vib,O_2}}}$	T	16	$O_2^+ + N_2$	$\rightleftarrows$	$N_2^+ + O_2$	T	T
5	$O_2 + M_2$	$\rightleftarrows$	$O + O + M_2$	$\sqrt{T \cdot T_{\mathrm{vib,O_2}}}$	T	17	$O_2^+ + O$	$\rightleftarrows$	$O^+ + O_2$	T	T
6	$NO + M_3^c$	$\rightleftarrows$	$N + O + M_3$	$\sqrt{T \cdot T_{\mathrm{vib,NO}}}$	T	18	$NO^+ + N$	$\rightleftarrows$	$O^+ + N_2$	T	T
7	$NO + M_4^d$	$\rightleftarrows$	$N + O + M_4$	$\sqrt{T \cdot T_{\mathrm{vib,NO}}}$	T	19	$NO^+ + O_2$	$\rightleftarrows$	$O_2^+ + NO$	T	T
8	$N_2 + O$	$\rightleftarrows$	$NO + N$	T	T	20	$NO^+ + O$	$\rightleftarrows$	$O_2^+ + N$	T	T
9	$NO + O$	$\rightleftarrows$	$N + O_2$	T	T	21	$O^+ + N_2$	$\rightleftarrows$	$N_2^+ + O$	T	T
10	$N + O$	$\rightleftarrows$	$NO^+ + e^-$	T	T	22	$NO^+ + N$	$\rightleftarrows$	$N_2^+ + O$	T	T
11	$N + N$	$\rightleftarrows$	$N_2^+ + e^-$	T	T	23	$N + e^-$	$\rightleftarrows$	$N^+ + e^- + e^-$	T_e	T_e
12	$O + O$	$\rightleftarrows$	$O_2^+ + e^-$	T	T	24	$O + e^-$	$\rightleftarrows$	$O^+ + e^- + e^-$	T_e	T_e

[a] $M_1 = N_2, O_2, NO, N_2^+, O_2^+, NO^+$
[b] $M_2 = N, O, N^+, O^+$
[c] $M_3 = N_2, O_2, N_2^+, O_2^+$
[d] $M_4 = NO, N, O, NO^+, N^+, O^+$

2.6 Radiation Calculation

The VSL analysis is not coupled with the calculation of radiative heat transfer. Radiation analysis is performed by SPRADIAN (Fujita & Abe 1997) in a non-coupled manner, using the numerical results. In the estimation of radiative heat flux, a spherical cap model (Fujita & Abe 1997) is used for the integration of the heat transfer equation. Emission and absorption of radiation are not considered in the VSL calculation.

3. RESULTS AND DISCUSSION

Figures 4 and 5 show temperatures and species mole fractions on the stagnation stream line for NCW at the altitude of 84 km, respectively. The horizontal axis is normalized by the shock distance y_{sh} that is 2.07 cm at this altitude. Immediately behind the shock, the translational-rotational temperature is elevated up to 58,000 K. Vibrational temperature of N_2 ($T_{\mathrm{vib,N_2}}$) slowly increases towards wall and then decreases near the wall. Electron temperature is raised rapidly immediately behind the shock because of high thermal conductivity of electron. Electron temperature is getting closer to equilibration with $T_{\mathrm{vib,N_2}}$ because of the strong coupling of nitrogen vibration and electron. Vibrational temperature of O_2 ($T_{\mathrm{vib,O_2}}$) is suppressed relatively low under 3,400 K. Since the degree of nonequilibrium is strong at this altitude, the vibrational energy loss of O_2 which is accompanied by dissociation is relatively large compared with the gain due to energy exchange. NO vibrational temperature ($T_{\mathrm{vib,NO}}$) indicates an almost constant value through the shock layer. As for the chemical reaction, it is seen in Fig. 5 that the dissociation of O_2 is active and the recombination reactions are not remarkable even near the wall.

The results for the altitude of 64 km are illustrated in Figs. 6 to 8. Figure 6 shows the temperatures on the stagnation stream line for NCW. The shock distance is 1.26 cm at this

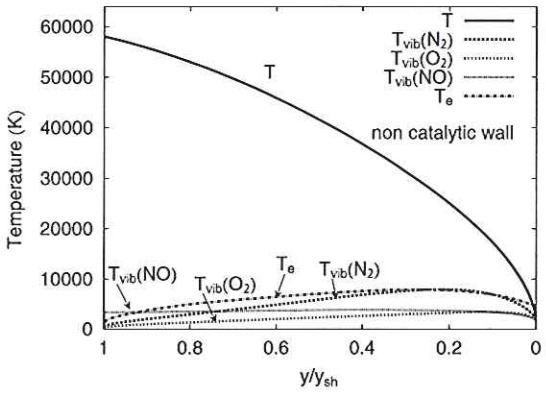

Fig. 4: On-axis temperatures at 84 km for NCW.

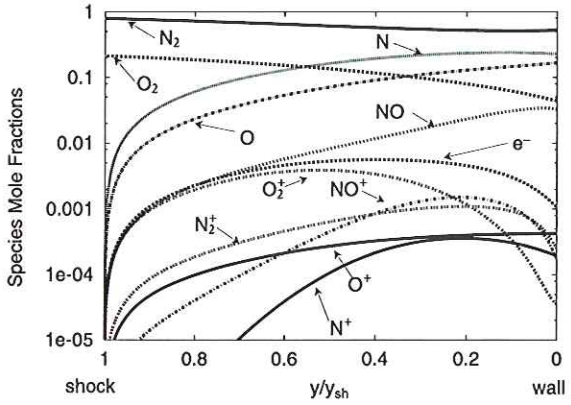

Fig. 5: On-axis species mole fractions at 84 km for NCW.

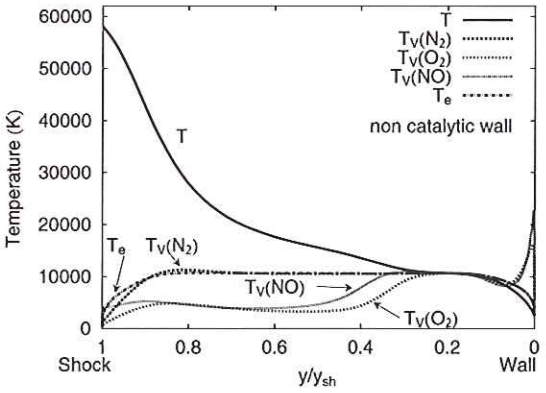

Fig. 6: On-axis temperatures at 64 km for NCW.

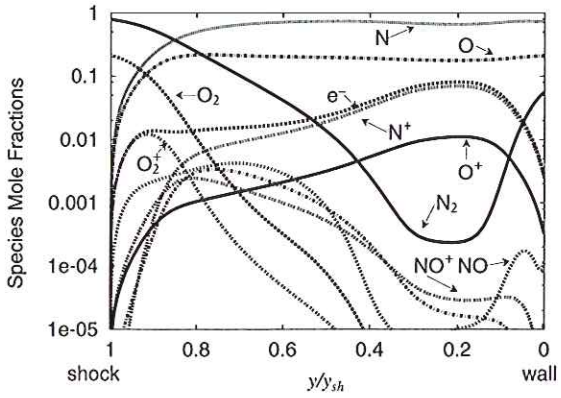

Fig. 7: On-axis species mole fractions at 64 km for NCW.

altitude. T_e and T_{vib,N_2} are close to each other except for immediately behind the shock. T_{vib,O_2} and $T_{vib,NO}$ are suppressed under 4,000 K from the shock to the middle of the shock layer because of large vibrational energy removal due to strong dissociation. As shown in Fig. 7, the mole fraction of electron increases in the region which is attributed to "Avalanche Ionization". The adoption of the multi vibrational temperature model changes dissociation rates, whereby N_2 dissociation becomes more active than that in the three temperature model composed of translational-rotational, vibrational and electron temperatures. On the other hand, O_2 dissociation gets weak compared with that in the three temperature model. Increases in T_{vib,O_2} and $T_{vib,NO}$ are observed in the vicinity of the wall. However, such a temperature elevation near the wall does not appear in the case of FCW as shown in Fig. 8.

Figure 9 shows radiation spectra at the stagnation point at the altitude of 64 km for NCW. The intensities of UV and VUV spectra observed at the stagnation point are extremely large because of the disappearance of O_2 which absorbs such spectra. The dashed line is the spectra calculated from the solution for the three temperature model (3T model). Radiative heat flux estimated from the analysis using the multi vibrational temperature model is 0.94 MW/m^2 while it is 0.96 MW/m^2 for the three temperature model.

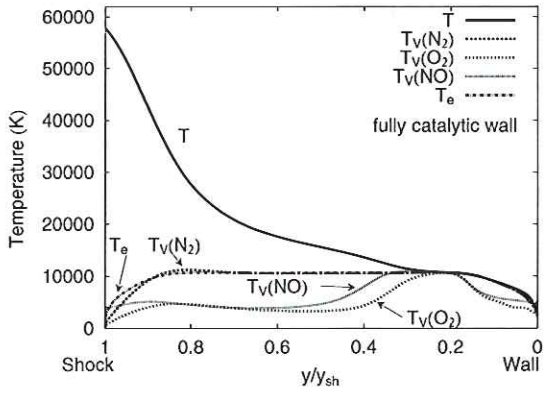

Fig. 8: On-axis temperature at 64 km for FCW.

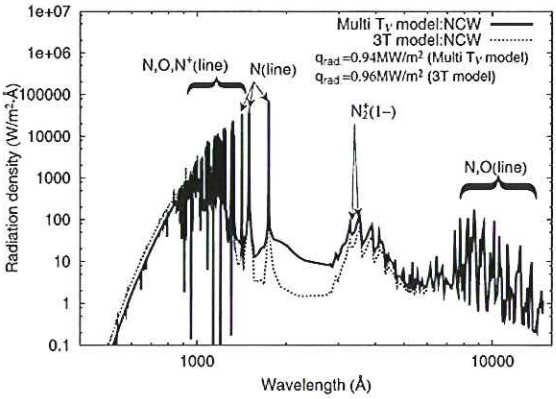

Fig. 9: Stagnation point radiation spectra at 64 km for NCW.

Table 2: Stagnation point convective heat flux (unit: MW/m^2).

Catalytic wall condition	NCW			FCW		
Altitude	74 km	64 km	54 km	74 km	64 km	54 km
q_w for a 3 temp. model	3.0	4.4	6.1	5.0	7.5	8.2
q_w for a multi vib. temp. model	2.4	3.4	6.1	5.0	7.5	7.8

The band spectra of $N_2^+(1-)$ are more intense because T_{vib,N_2} is larger than T_{vib} from the three temperature model analysis. However the line spectra from atoms become weak because T_e slightly decreases compared with that in the three temperature model analysis. Since the energy coupling of N_2 and electron is very strong, distinguishing each vibrational temperature influences electron temperature. In addition, the shock distance in the multi vibrational temperature model analysis slightly decreases compared with that from the three temperature model because the degree of dissociation has changed as mentioned above. Thus, radiation volume decreases. Nevertheless, as a result, total radiative heat flux is decreased by 2.3 % from the three temperature analysis. In the present analysis, vibrational temperatures of molecular ion species are set to being equal to those of corresponding neutral species. If the vibrational temperature of such ion molecule is individually considered, the radiative heat flux might change, because radiation from N_2^+ is very intense compared with that from N_2. The effect of the vibrational temperature of ion molecules is a future problem to be solved.

In Table 2 is given a comparison of stagnation point convective heat fluxes for a three temperature model and a multi vibrational temperature model at three altitudes. In the case of NCW, the convective heat flux at the altitude of 74km and 64 km is less than the results from the three temperature model. In case of FCW, the convective heat flux at the altitude of 54 km is also less that that from the three temperature model. Overall, the adoption of the multi vibrational temperature model appears to decrease convective and radiative heat fluxes.

4. CONCLUDING REMARKS

The nonequilibrium shock layer over the super orbital reentry capsule of MUSES-C has been numerically analyzed by using the thermochemical nonequilibrium viscous shock layer equations with a multi vibrational temperature model. As shown above, the behavior of vibrational temperature of individual molecular species has been revealed.

The radiation analysis has shown a slight decrease in radiative heat flux from that for the three temperature model. However, the convective heat flux are partly much less than that from the three temperature model analysis.

REFERENCES

Candler, G.V., MacCormack, R.W., 1991, Computation of weakly ionized hypersonic flows in thermochemical nonequilibrium, J. Thermophys. Heat Transfer, Vol. 5, pp. 266–273.

Curtiss, C.F., Hirschfelder, J.O., 1949, Transport properties of multi component gas mixture, J. Chem. Phys., Vol. 17, pp. 550–555.

Doihara, R., Nishida, M., 2001, The VSL analysis of the flow field over a super orbital reentry capsule Transactions of the Japan Society for Aeronautics and Space Science, Vol. 44, pp. 73–81.

Doihara, R., Nishida, M., 2002, Thermochemical nonequilibrium viscous shock layer studies of the orbital reentry experiment (OREX) vehicle, Shock Waves, Vol. 11, pp. 331–339.

Fujita, K., Abe, T., 1997, SPRADIAN, Structured package for radiation analysis: theory and application, Institute of Space and Astronautical Science, Sagamihara, Japan, ISAS Report 669.

Gupta, R.N., Lee, K.P., Zoby, E.V., Moss, J.N., Thompson, R,A., 1990a, Hypersonic viscous shock-layer solutions over long slender bodies - Part I: High Reynolds number flows, J. Spacecraft, Vol. 27, pp. 175–184.

Gupta, R.N., Lee, K.P., Zoby, E.V., Moss, J.N., Thompson, R.A., 1990b, Hypersonic viscous shock-layer solutions over long slender bodies - Part II: Low Reynolds number flows, J. Spacecraft, Vol. 27, pp. 185–193.

Gupta, R.N., Yos, J.M., Thompson, R.A., Lee, K.P., 1990c, A review of reaction rates and thermodynamic and transport properties for an 11-species air model for chemical and thermal nonequilibrium calculations to 30000K, NASA RP-1232.

Gupta, R.N., 1996, Viscous shock-layer study of thermochemical nonequilibrium, J. Thermophys. Heat Transfer, Vol. 10, pp. 257–266.

Gupta, R.N., Moss, J.N., Price, J.M., 1996, Assessment of thermochemical nonequilibrium and slip effects for orbital reentry experiment (OREX), AIAA Paper 96-1859.

Lazdinis, S.S., Petrie, S.L., 1974, Free electron and vibrational temperature nonequilibrium in high temperature nitrogen, Phys. Fluids, Vol. 17, pp. 1539–1546.

Lee, J.H., 1985, Basic governing equations for the flight regimes of aeroassisted orbital transfer vehicles, AIAA Progress in Astronautics and Aeronautics, Vol.96, New York, pp. 3–53.

Lee, J.H., 1992, Electron-impact vibrational relaxation in high-temperature nitrogen, AIAA Paper 92-0807.

Millikan, R.C., White, D.R., 1963, Systematics of vibrational relaxation, J. Chem. Phys., Vol. 139, pp. 34–43.

Miner, E.W., Lewis, C.H., 1975, Hypersonic ionizing air viscous shock-layer flows over nonanalytic blunt bodies, NASA CR-2550 (1975)

Nishida, M., 1972, Nonequilibrium viscous shock layer in a partially ionized gas, Phys. Fluids, Vol. 15, pp. 596–602.

Nishida, M., Sakamura, Y., 1994, Nonequilibrium viscous shock layer analysis using a three temperature model, AIAA Progress in Astronautics and Aeronautics Vol. 158, pp. 401–412.

Park, C., 1985, Problems of rate chemistry in the flight regimes of aeroassisted orbital transfer vehicles, AIAA Progress in Astronautics and Aeronautics, Vol. 96, pp. 511–537.

Park, C., 1990, Nonequilibrium Hypersonic Aerothermodynamics (John Wiley & Sons, Inc. New York).
Park, C., 1993, Review of chemical-kinetic problems of future NASA missions. I:earth entries, J. Thermophys. Heat Transfer, Vol. 7, pp. 385–398.
Sakamura, Y., Nishida, M., 1991, Numerical calculation of thermal and chemical nonequilibrium flows around a hypersonic reentry vehicle. Trans. Japan Soc. Aero. Space Sci., Vol. 34, pp. 27–45.
Suzuki, K., Kubota, H., Fujita, K., Abe, T, 1996, Numerical analysis of aerodynamic heating on MUSES-C reentry capsule, Proc. 20th International Symposium on Space Technology and Science, Gifu, Japan, ISTS 96-d-25.
Treanor, C.E., Marrone, P.V., 1962, Chemical relaxation with preferential dissociation from excited vibrational level, Phys. Fluids, Vol. 5, 1022.